Asymptotic analysis of stresses near a crack tip in a two dimensional colloidal packing saturated with liquid*

Arijit Sarkar Mahesh S Tirumkudulu †

November 23, 2010

Abstract

The consolidation of colloidal particles in drying colloidal dispersions is influenced by various factors such as particle size and shape, and inter-particle potential. The capillary pressure induced by the menisci, formed between the top layer of particles in the packed bed, compresses the bed of particles while the constraints enforced by the boundaries result in tensile stresses in the packing. Presence of flaws or defects in the bed determines its ultimate strength under such circumstances. In this study, we determine the asymptotic stress distribution around a flaw in a two dimensional colloidal packing saturated with liquid and compare the results with those obtained from the full numerical solution of the problem. Using the Griffith's criterion for equilibrium cracks, we relate the critical capillary pressure at equilibrium to the crack size and the mechanical properties of the packed bed. The analysis also gives the maximum allowable flaw size for obtaining a crack free packing.

*Currently under review in *Langmuir*

†Department of Chemical Engineering, Indian Institute of Technology-Bombay, Powai, Mumbai 400076, India: arijit@che.iitb.ac.in; mahesh@che.iitb.ac.in

1 Introduction

Dried colloidal particle films find use in a number of applications such as tapes for photography and magnetic storage[1], porous coated printer papers, coating vitamin tablets, synthetic opals, photonic crystals[2] etc. The macroscopic properties of the film such as its thickness, particle packing and the mechanical strength are influenced by the drying rate, interparticle potential, particle size and shape and the modulus of the particles. When a dispersion of colloidal particles is dried, the particles concentrate, eventually reaching a close packed concentration. The liquid menisci on the top layer of particles compresses the packing while the substrate resists transverse deformation of the packing. Consequently, transverse tensile stresses develop in the packing and when these stresses exceed a critical value, the packing cracks resulting in a variety of crack patterns. Such cracks occur not only in thin films such as paints and coatings but also in thick systems and over geophysical length scales such as in the case of dried river beds.

Most of the experimental investigations of the cracking phenomenon in drying colloidal dispersions have focused on the thin film geometry where stresses have been measured using the classical cantilever bending technique.[1,3,4] These measurements show that thin films of monodisperse colloidal dispersions containing identical particles crack at a critical stress that is independent of the particle size but varies inversely with the film thickness.[5,6,3,7] In almost all cases, the film nucleates multiple cracks with crack spacing that varies linearly with film thickness.[3,8] Experiments also suggest that irrespective of particle size or moduli, each dispersion has a maximum crack free thickness below which the films do not crack. The critical cracking thickness is found to increase with particle size and moduli in the case of hard polymer and metal oxide particles. A number of investigations have also focused on cracking in confined geometries such as capillary tubes where the dispersion dries from one end resulting in a compaction front of packed particles. While direct measurement of stresses has not been possible in this geometry, the studies have focused on crack tip velocity and

its relation to the speed of the compaction front.[9,10,11]

On the theoretical front, Routh and Russel[12] have derived a constitutive relation relating the macroscopic stress to macroscopic strain in a drying film. They considered the viscoelastic deformation of a pair of identical particles due to contact and interfacial forces and related the strain at the particle level to these forces. Next, they volume averaged the forces over all orientations to arrive at the macroscopic stress versus strain relationship for a drying film. In the absence of particle-solvent interfacial tension, the expression for the macroscopic stress tensor[3] for identical elastic spheres reduces to

$$\sigma_{ij} = \delta_{ij}\left\{-P - \frac{GM\phi_{rcp}}{140}\left(\epsilon_{mm}^2 + 2\epsilon_{nm}\epsilon_{mn}\right)\right\} - \frac{GM\phi_{rcp}}{35}\left(\epsilon_{mm}\epsilon_{ij} + 2\epsilon_{im}\epsilon_{mj}\right) \qquad (1)$$

where, ϵ_{ij} is the macroscopic strain, P is the capillary pressure, ϕ_{rcp} is the random close packing concentration, G is the shear modulus of the particles and M is the number of contacting neighbors. The constitutive equation is an improvement over the traditional poroelasticity models[13,14,15] as the former accounts for the nonlinear deformation at the particle level and the influence of particle size, modulus and packing characteristics on the macroscopic deformation field. The model has been successful in predicting not only the stress profile in drying films of both film forming and cracking systems,[16] but also in predicting many aspects of the cracking mechanism in the latter.[3] More recently, Russel et. al.[17] have improved on the above relation by adopting the Hertzian contact mechanics at the particle pair level. The final constitutive relation is also non-linear where the stress varies as three halves power of the strain. Using this relation, they determine the capillary pressure necessary either to open an infinite crack in a flawless film or to extend pre-existing flaws of finite lengths. Their results suggest that flaws which are a fraction of the film thickness are sufficient to initiate cracks that would propagate across the sample at pressures modestly greater than obtained from the energy argument. In a related study Man and Russel[18] demonstrate experimentally the role of flaws in nucleating cracks and show that the critical stress obtained from the energy argument only gives the lower

bound.

In this study, we determine the stress field near a crack tip along with the shape of the crack that is present in a particle packing saturated with solvent. A packed bed made of an array of colloidal particles can be considered to be a collection of polycrystalline aggregates with pre-existing flaws. These flaws may be attributed to micro-cracks, grain boundaries between the clusters of ordered packing of monodispersed particles, dissimilar pores inside the colloidal bed etc. Nucleation of crack under these circumstances changes the stress field close to the crack with stress concentration at the crack tip. The stress and strain fields are linearized about the pre-crack state to determine the disturbance displacement field immediately after the opening of a mode-I crack. These results also yield the stress intensity factor for the two dimensional elastic field which is then related to the surface energy using the well known Griffith's criterion for equilibrium cracks. The calculated quantities are then compared with the numerical solution for the full problem. The calculations show that the dimensionless critical capillary pressure required to open a crack varies inversely with the crack length to the two thirds' power and depends on a dimensionless parameter that measures the ratio of the elastic to surface energy. A simple scaling analysis reveals the essence of the results to follow. Since $\sigma \sim E\epsilon^{o2}$, where '$E$' is effective modulus of the packing and ϵ^o is the characteristic strain in the packing, the elastic energy recovered on the opening of a crack of length 'a' in a packing of unit thickness is, $\sigma\epsilon^o a^2$. Equating this to surface energy (γa) and noting that the capillary pressure is linearly related to the stress, gives the critical capillary pressure for opening the crack, $\frac{P_c R}{2\gamma} \sim A\left(\frac{R}{a}\right)^{2/3}\left(\frac{ER}{\gamma}\right)^{1/3}$, where '$\gamma$' is the surface tension of the solvent, R is the radius of the particles, and A is a constant. The objective of this paper is to rigorously determine the value of A and investigate the consequence of this result.

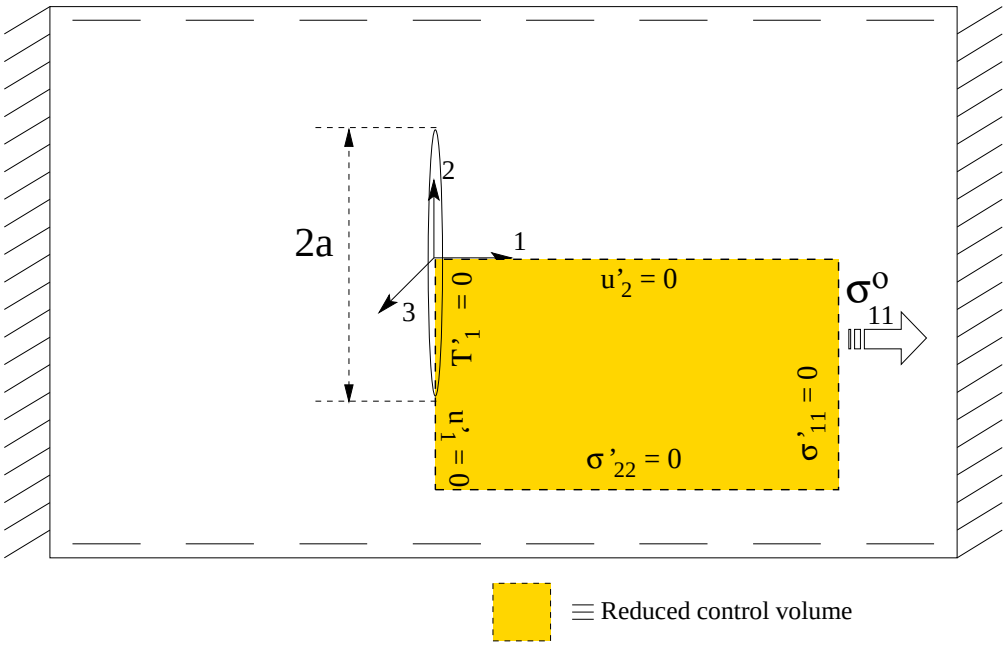

Figure 1: A crack of length $2a$ embedded in a packed bed. The bed is stressed in '1' direction. Shaded region shows the region over which the analysis is performed. T_1' is the traction along crack surface.

2 Nucleation of crack

Consider a two dimensional packed bed of colloidal particles that is initially stressed by capillary pressure. The bed is stressed in the x_1 direction so that it is free to expand along x_2 and x_3 (Figure 1). In this case, the strain is given by, $\epsilon_{ij} = -\epsilon^o\left(\delta_{i2}\delta_{2j} + \delta_{i3}\delta_{3j}\right)$, where ^{o} denotes the pre-crack values. Volume conservation over a unit volume of the bed relates the strain to the particle volume fraction,

$$\phi^o = \phi\left(1-\epsilon^o\right)^2 . \tag{2}$$

where, ϕ^o is the volume fraction in the pre-crack state. A crack of dimensionless length $2a$ nucleates along x_2 and changes the stress and strain field in the sample,

$$\epsilon_{ij} = -\epsilon^o\left(\delta_{i2}\delta_{2j} + \delta_{i3}\delta_{3j}\right) + \epsilon'_{ij} \;\;,\;\; P = P^o + P' \;\text{ and, }\; \sigma_{ij} = \sigma^o_{ij} + \sigma'_{ij}, \tag{3}$$

with the perturbed variables represented by the primed quantities. Substituting these in the constitutive equation (1) and retaining terms linear in the perturbed quantities

gives,

$$\begin{aligned}
\bar{\sigma'}_{11} &= -\bar{P'} + (3\epsilon'_{11} + 2\epsilon'_{22} + 2\epsilon'_{33}) \\
\bar{\sigma'}_{22} &= -\bar{P'} + (2\epsilon'_{11} + 9\epsilon'_{22} + 3\epsilon'_{33}) \\
\bar{\sigma'}_{33} &= -\bar{P'} + (2\epsilon'_{11} + 3\epsilon'_{22} + 9\epsilon'_{33}) \\
\bar{\sigma'}_{12} &= 4\epsilon'_{12} \\
\bar{\sigma'}_{23} &= 6\epsilon'_{23} \\
\bar{\sigma'}_{31} &= 4\epsilon'_{31}
\end{aligned} \tag{4}$$

where a bar over a variable implies a dimensionless quantity with stress and pressure rendered dimensionless with $E \equiv \frac{GM\phi_{rcp}\epsilon^o}{35}\cdot$ The dimensionless stress for the pre-crack state is,

$$\bar{\sigma^o}_{ij} = \delta_{ij}\left[-\bar{P}^o - 2(\epsilon^o)\right] - 4(\epsilon^o)\left(\delta_{i2}\delta_{2j} + \delta_{i3}\delta_{3j}\right)\cdot \tag{5}$$

Since we consider the plane stress case ($\bar{\sigma}_{3j} = 0$) and the bed is stressed only in the x_1 direction, $\bar{P}^o = -6\epsilon^o$, $\bar{\sigma^o}_{11} = 4\epsilon^o$ and $\bar{\sigma^o}_{22} = 0$

Since the total amount of particle phase remains constant in the packing, the particle volume fractions before and after cracking are related,

$$\frac{\phi_{rcp}}{\phi} = (1 + \epsilon'_{11})(1 - \epsilon^o + \epsilon'_{22})(1 - \epsilon^o + \epsilon'_{33}) \tag{6}$$

where, ϕ_{rcp} is the random close packing and the strain is taken to be zero when $\phi = \phi_{rcp}$. The time evolution of stress and strain around the crack can be further subdivided into two limiting cases i.e. the short time and the long time limits. In the short time limit, the impact of crack formation on the stress and strain variation is such that it would occur in the absence of solvent flow, suggesting that the material will be incompressible. Thus, in the short time limit and for $\epsilon^o \ll 1$, (6) reduces to,

$$\epsilon'_{11} + \epsilon'_{22} + \epsilon'_{33} = 0. \tag{7}$$

Since we shall consider only the plane stress case here ($\bar{\sigma'}_{33} = 0$), $\bar{P'} = \epsilon'_{22} + 7\epsilon'_{33}$. At longer time scales, liquid flows so as to eliminate pressure variations, giving us the

required condition for the long time limit, $\bar{P}' = 0$. The perturbed stress and strain are compactly related in the two cases, $\bar{\sigma'}_{ij} = C_{ij}\epsilon^{e\prime}_{ij}$ where $\epsilon^{e\prime}_{ij}$ is the engineering strain and C is the stiffness matrix. The latter is given by,

$$C = \begin{bmatrix} 8 & 6 & 0 \\ 6 & 12 & 0 \\ 0 & 0 & 2 \end{bmatrix} \tag{8}$$

in the short-time limit and,

$$C = \begin{bmatrix} \frac{23}{9} & \frac{4}{3} & 0 \\ \frac{4}{3} & 8 & 0 \\ 0 & 0 & 2 \end{bmatrix} \tag{9}$$

in the long-time limit. While the stress field in the pre-crack stress (1) is nonlinear but isotropic, (8) and (9) suggest it becomes anisotropic in the perturbed state. For convenience we write the constitutive equations as, $\Delta_i = S_{ij}\Sigma_j$ where the components of Δ and Σ are given by, $\epsilon^{e\prime}_{11}, \epsilon^{e\prime}_{22}, \epsilon^{e\prime}_{33}, \epsilon^{e\prime}_{23}, \epsilon^{e\prime}_{31}, \epsilon^{e\prime}_{12}$ and $\bar{\sigma'}_{11}, \bar{\sigma'}_{22}, ..., \bar{\sigma'}_{12}$ respectively, and the elements of $\mathbf{S}$ are determined from $\mathbf{C}$. Note that the present case relates to the case of a orthotropic anisotropy with plane stress condition. Therefore, $\mathbf{S}$ has only seven non-zero elements. The displacement field in case of plane strain is easily obtained using the procedure outlined in the next section except that the components of the stiffness matrix for the plane stress problem (S_{ij}) are replaced with,

$$D_{ij} = S_{ij} - \frac{S_{i2}S_{j3}}{S_{33}}, \quad (i, j = 1, 2, ..., 6)$$

for the plane strain case.

3 Asymptotic analysis near a crack tip

The knowledge of the stress fields in the neighborhood of the crack tip is essential in determining the strength of the packed bed. Since the perturbed stress is linear in perturbed strain, we draw upon the mathematical techniques developed in the solid

mechanics literature to determine the stress field near the tip of a crack.[19,20,21,22,23] The coordinate system $(\tilde{x}_1, \tilde{x}_2)$ for this analysis is shown in Figure 1 where the origin is placed at the crack tip so that $\tilde{x}_1 = \bar{x}_1, \tilde{x}_2 = \bar{x}_2 + \bar{a}$ and the variables have been rendered dimensionless using the characteristic length of the solution domain. The momentum balance equation in $\tilde{x}_1$ and $\tilde{x}_2$ directions in the absence of body forces are given by,

$$\begin{aligned} \frac{\partial \bar{\sigma'}_{11}}{\partial \tilde{x}_1} + \frac{\partial \bar{\sigma'}_{12}}{\partial \tilde{x}_2} = 0, \text{ and} \\ \frac{\partial \bar{\sigma'}_{21}}{\partial \tilde{x}_1} + \frac{\partial \bar{\sigma'}_{22}}{\partial \tilde{x}_2} = 0. \end{aligned} \tag{10}$$

Following Sih et al.[19] and Hoenig[24], we related stresses to stress correlation functions, χ and ψ,

$$\begin{aligned} \bar{\sigma'}_{ij} &= -\frac{\partial^2 \chi}{\partial \tilde{x}_i \partial \tilde{x}_j} + \delta_{ij} \frac{\partial^2 \chi}{\partial \tilde{x}_m^2} \\ \bar{\sigma'}_{3i} &= e_{ij} \frac{\partial \psi}{\partial \tilde{x}_j} \end{aligned} \tag{11}$$

with e_{ij} and δ_{ij} being the second order alternating and Dirac delta tensor respectively, and i, j allowed values of 1 or 2. Note that (11) automatically satisfies (10). The above expressions along with the constitutive relation are substituted in the compatibility equations,

$$\begin{aligned} \frac{\partial^2 \epsilon^{e\prime}_{11}}{\partial \tilde{x}_2^2} + \frac{\partial^2 \epsilon^{e\prime}_{22}}{\partial \tilde{x}_1^2} - \frac{\partial^2 \epsilon^{e\prime}_{12}}{\partial \tilde{x}_1 \partial \tilde{x}_2} = 0, \text{ and} \\ \frac{\partial^2 \epsilon^{e\prime}_{11}}{\partial \tilde{x}_2 \partial \tilde{x}_3} = \frac{\partial^2 \epsilon^{e\prime}_{12}}{\partial \tilde{x}_3 \partial \tilde{x}_1} - \frac{\partial^2 \epsilon^{e\prime}_{23}}{\partial \tilde{x}_1^2} + \frac{\partial^2 \epsilon^{e\prime}_{31}}{\partial \tilde{x}_1 \partial \tilde{x}_2} \end{aligned} \tag{12}$$

to give, respectively,

$$S_{11}\chi_{,2222} + (2S_{12} + S_{66})\chi_{,1122} + S_{22}\chi_{,1111} = 0, \quad \text{and} \tag{13}$$

$$S_{44}\psi_{,11} + S_{55}\psi_{,22} = 0. \tag{14}$$

The degree of anisotropy in the material can be judged by rewriting (13) differently,

$$\nabla^4 \chi + \delta_1 \chi_{,1111} + \delta_2 \chi_{,2222} = 0 \tag{15}$$

where $1+\delta_1 = \frac{2S_{22}}{S_{66}+2S_{12}}$ and $1+\delta_2 = \frac{2S_{11}}{S_{66}+2S_{12}}$ are indicators of anisotropy in the material. The difference in the values of δ_1 and δ_2 originate from the fact that the bed is held along '1' direction and perturbed along '2' and '3' directions leading to a directional perturbation of the stress field. When $|\delta_i| \ll 1$, χ satisfies the biharmonic equation, i.e. the material is isotropic. In the current problem, δ_i are -0.12 and 0.33 in the short-time limit and -0.24 and 1.4 in the long-time limit suggesting that the anisotropy is significant and cannot be ignored.

(13) and (14) are a pair of decoupled equations in χ and ψ,

$$L_4\chi = 0 \tag{16}$$

$$L_2\psi = 0 \tag{17}$$

where the differential operators are given by, $L_2 \equiv S_{44}\frac{\partial^2}{\partial\tilde{x}_1^2} + S_{55}\frac{\partial^2}{\partial\tilde{x}_2^2}$ and $L_4 \equiv S_{11}\frac{\partial^4}{\partial\tilde{x}_2^4} + 2(S_{12}+S_{66})\frac{\partial^4}{\partial\tilde{x}_1^2\partial\tilde{x}_2^2} + S_{22}\frac{\partial^4}{\partial\tilde{x}_1^4}$. Lekhnitskii[20] has shown that L_2 and L_4 can be decomposed into two and four linear operators of first order respectively, of the form $D_k = \partial/\partial\tilde{x}_2 - \mu_k\partial/\partial\tilde{x}_1$ such that $D_1D_2D_3D_4\chi = 0$ and $D_5D_6\psi = 0$. Substitution of D_k in L_4 and L_2 shows that μ_k are roots of the polynomial operators, $l_4 \equiv S_{11}\mu_k^4 + (2S_{12}+S_{66})\mu_k^2 + S_{22} = 0$ and $l_2 \equiv S_{55}\mu_k^2 + S_{44} = 0$. Then, the stress correlation functions can be written as,

$$\begin{aligned} \chi &= \sum_{i=1}^{2}\{\chi_i(\tilde{x}_1+\mu_i\tilde{x}_2) + \chi_i(\tilde{x}_1+\bar{\mu}_i\tilde{x}_2)\} \quad \text{and} \\ \psi &= \psi(\tilde{x}_1+\mu_i\tilde{x}_2) + \psi(\tilde{x}_1+\bar{\mu}_i\tilde{x}_2) \end{aligned} \tag{18}$$

where the bar on μ_i represents the conjugate complex number. Further, Lekhnitskii[20] has shown that for the elastic energy of the packing to be positive, the roots cannot be real. Consequently, the general expression for the stress function will involve the real part of both the complex conjugates,

$$\begin{aligned} \chi_R(\tilde{x}_1,\tilde{x}_2) &= 2\,\mathbf{Re}\left\{\sum_{i=1}^{2}\chi_i(z_i)\right\} \\ \psi_R(\tilde{x}_1,\tilde{x}_2) &= 2\,\mathbf{Re}\{\psi(z_3)\} \end{aligned} \tag{19}$$

where $z_i = \tilde{x}_1 + \bar{\mu}_i\tilde{x}_2$ and **Re** represents the real part. Since the stresses are related to the derivatives of the above functions, it is convenient to assume the following

functional form,

$$\frac{\partial \chi_k(z_k)}{\partial z_k} = G_k(z_k) \text{ for } k \in [1,2]$$
$$\text{and} \qquad \psi_3(z_3) = G_3(z_3) \tag{20}$$

so that the definition of stresses are given by,

$$\begin{aligned}
\bar{\sigma'}_{11} &= \frac{\partial^2 \chi_R}{\partial \tilde{x}_2^2} = 2\,\mathbf{Re}\left[\mu_1^2 \frac{\mathrm{d}G_1}{\mathrm{d}z_1} + \mu_2^2 \frac{\mathrm{d}G_2}{\mathrm{d}z_2}\right], \\
\bar{\sigma'}_{22} &= \frac{\partial^2 \chi_R}{\partial \tilde{x}_1^2} = 2\,\mathbf{Re}\left[\frac{\mathrm{d}G_1}{\mathrm{d}z_1} + \frac{\mathrm{d}G_2}{\mathrm{d}z_2}\right], \\
\bar{\sigma'}_{12} &= -\frac{\partial^2 \chi_R}{\partial \tilde{x}_1 \partial \tilde{x}_2} = -2\,\mathbf{Re}\left[\mu_1 \frac{\mathrm{d}G_1}{\mathrm{d}z_1} + \mu_2 \frac{\mathrm{d}G_2}{\mathrm{d}z_2}\right], \\
\bar{\sigma'}_{31} &= \frac{\partial \psi_R}{\partial \tilde{x}_2} = 2\,\mathbf{Re}\left[\mu_3 \frac{\mathrm{d}G_3}{\mathrm{d}z_3}\right], \\
\text{and, } \bar{\sigma'}_{23} &= -\frac{\partial \psi_R}{\partial \tilde{x}_1} = -2\,\mathbf{Re}\left[\frac{\mathrm{d}G_3}{\mathrm{d}z_3}\right].
\end{aligned} \tag{21}$$

We can also determine the strain components in terms of the stress function, for example,

$$\epsilon_{11}^{e\prime} = \frac{\partial \bar{u}_1'}{\partial \tilde{x}_1} = 2\,\mathbf{Re}\left[\frac{\mathrm{d}G_1}{\mathrm{d}z_1}(S_{11}\mu_1^2 + S_{12} - S_{16}\mu_1) + \frac{\mathrm{d}G_2}{\mathrm{d}z_2}(S_{11}\mu_2^2 + S_{12} - S_{16}\mu_2)\right].$$

Integrating the above expression with respect to z_j gives the displacement field in the '1' direction,

$$\bar{u}_1' = 2\,\mathbf{Re}\left\{\sum_{j=1}^{2} p_{1j} G_j(z_j)\right\} \quad \text{where} \quad p_{1j} = S_{11}\mu_j^2 + S_{12} - S_{16}\mu_j.$$

Following a similar procedure for the remaining strain components, all displacements are determined,

$$\bar{u}_i' = 2\,\mathbf{Re}\left\{\sum_{j=1}^{3} p_{ij} G_j(z_j)\right\} \tag{22}$$

where

$$\begin{aligned}
p_{1i} &= S_{11}\mu_i^2 + S_{12} - S_{16}\mu_i \\
p_{2i} &= S_{12}\mu_i + S_{22}/\mu_i - S_{26} \\
p_{33} &= S_{45} - S_{44}/\mu_3 \\
p_{31} &= p_{32} = p_{13} = p_{23} = 0
\end{aligned} \tag{23}$$

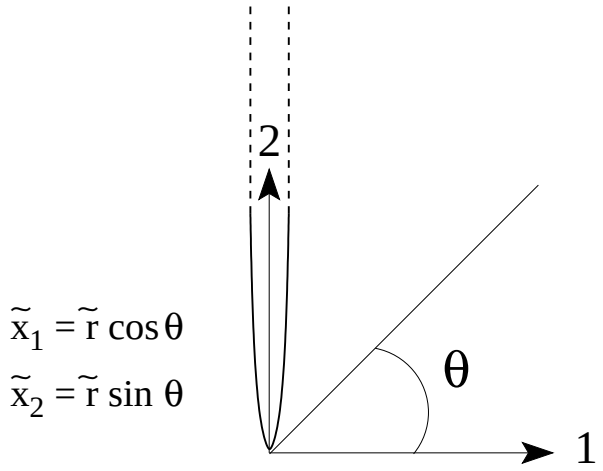

Figure 2: Shifted coordinate system for the asymptotic analysis

Next, we ascertain the functional form of G_i. Rice[21] has shown that the J-integral, $J = \int_{\mathrm{d}\Omega} \left(W \mathrm{d}\tilde{x}_1 - \bar{\sigma'}_{ij} n_j \frac{\mathrm{d}\bar{u}_i}{\mathrm{d}\tilde{x}_2} \mathrm{d}S \right)$, has the same value for all integration paths surrounding crack tips in two dimensional fields of linear or nonlinear elastic materials. Here, W is the strain energy density, n_j is the normal to the chosen path, and S is the distance along the path $\mathrm{d}\Omega$. Assuming $\frac{\mathrm{d}G_i}{\mathrm{d}z_i} \propto {z_i}^p$ in the neighbourhood of the crack opening, $W \propto {z_i}^{2p}$ and $\bar{\sigma'}_{ij} n_j \frac{\mathrm{d}\bar{u}_i}{\mathrm{d}\tilde{x}_2} \sim {z_i}^{2p}$. Hence, $J \sim {z_i}^{2p+1}$. Since the value of J should be independent of the path, $p = -\frac{1}{2}$. Thus, we assume $G = B_i \sqrt{2\bar{a} z_i / \pi}$ for a flaw of size $\bar{a}$ where B_i is the stress function amplitude. For a stress free crack

surface, the stress and displacement components near the crack tip become,

$$\begin{aligned}
\bar{\sigma'}_{11} &= \sqrt{\frac{2\bar{a}}{\pi\tilde{r}}}\,\mathbf{Re}\sum_{i=1}^{2}\frac{B_i\mu_i^2}{\sqrt{\cos\theta+\mu_i\sin\theta}},\\
\bar{\sigma'}_{22} &= \sqrt{\frac{2\bar{a}}{\pi\tilde{r}}}\,\mathbf{Re}\sum_{i=1}^{2}\frac{B_i}{\sqrt{\cos\theta+\mu_i\sin\theta}},\\
\bar{\sigma'}_{12} &= -\sqrt{\frac{2\bar{a}}{\pi\tilde{r}}}\,\mathbf{Re}\sum_{i=1}^{2}\frac{B_i}{\sqrt{\cos\theta+\mu_i\sin\theta}},\\
\bar{\sigma'}_{31} &= \sqrt{\frac{2\bar{a}}{\pi\tilde{r}}}\,\mathbf{Re}\,\frac{B_3\mu_3}{\sqrt{\cos\theta+\mu_3\sin\theta}},\\
\bar{\sigma'}_{23} &= -\sqrt{\frac{2\bar{a}}{\pi\tilde{r}}}\,\mathbf{Re}\,\frac{B_3}{\sqrt{\cos\theta+\mu_3\sin\theta}},\ \text{and}\\
\bar{u}'_i &= 2\sqrt{\frac{2\bar{a}\tilde{r}}{\pi}}\,\mathbf{Re}\sum_{j=1}^{3}p_{ij}B_j\sqrt{\cos\theta+\mu_j\sin\theta}.
\end{aligned}\tag{24}$$

Note that the perturbed normal stress at the crack surface for the current problem has a finite non-zero value ($-\bar{\sigma^o}_{11}$) which will require minor modifications to some of the above expressions and is dealt with towards the end of this section. The stress intensity factor (K) for mode I crack is defined as,

$$\bar{K}_1 = \mathbf{Re}\,\bar{K}_1 = \lim_{\substack{\tilde{x}_2\to 0^-\\ \tilde{x}_1=0}}\bar{\sigma'}_{22}\sqrt{2\pi\tilde{r}} = 2\sqrt{\bar{a}}\,\mathbf{Re}\sum_{i=1}^{2}\frac{B_i\mu_i^2}{\sqrt{-\mu_i}}\tag{25}$$

Similarly, $\bar{K}_2$ and $\bar{K}_3$ can be obtained from $\bar{\sigma'}_{12}$ and $\bar{\sigma'}_{13}$. Thus the stress intensity factor for the three modes can be written compactly,

$$\bar{\mathbf{K}} = -2\mathbf{i}\sqrt{\bar{a}}\mathbf{N}\mathbf{I}_\mu\mathbf{B}\tag{26}$$

where

$$[N] = \begin{bmatrix}\mu_1^2 & \mu_2^2 & 0\\ -\mu_1 & -\mu_2 & 0\\ 0 & 0 & \mu_3\end{bmatrix}\quad\text{and}\quad [I_\mu] = \begin{bmatrix}\frac{1}{\sqrt{\mu_1}} & 0 & 0\\ 0 & \frac{1}{\sqrt{\mu_2}} & 0\\ 0 & 0 & \frac{1}{\sqrt{\mu_3}}\end{bmatrix}.\tag{27}$$

The perturbed displacements of the crack surface can be found in terms of the distance from tip along the crack surface, $\theta\to\frac{\pi}{2}$, $\tilde{r}=\tilde{\zeta}$

$$\bar{\mathbf{u}}' = \mp\sqrt{\frac{2\tilde{\zeta}}{\pi}}\mathbf{Q}^{-1}\bar{\mathbf{K}}\tag{28}$$

where $\mathbf{Q^{-1}} = \mathbf{Im}\left\{\mathbf{pN^{-1}I_{\mu}^{-2}}\right\}$.

The above analysis gives the functional form of the stress and strain fields close to the crack tip in terms of the unknown $\bar{K}$. In order to determine the stress intensity factor, we assume a finite sized crack with an elliptical shape such that the minor axis of dimensionless length $2\bar{c}$ is small compared to the major axis ($2\bar{a}$), $\alpha = \frac{\bar{c}}{\bar{a}} \ll 1$. Eshelby[25] has shown that for an elliptical crack, the strain is uniform around the crack. Following Hoenig[24], the displacement of the crack surface is given by,

$$\bar{U}_i' = A_{1i}\bar{x}_1 = \beta_i\sqrt{\bar{a}^2 - \bar{x}_2^2} \text{ where, } \beta_i = \frac{A_{1i}}{\alpha},$$

and the strains by,

$$\epsilon_{11}^{e\prime} = \frac{\beta_1}{\alpha},\ \epsilon_{12}^{e\prime} = \frac{\beta_2}{2\alpha},\ \text{and } \epsilon_{13}^{e\prime} = \frac{\beta_3}{2\alpha}.$$

Thus, the perturbed stress at the crack face for this simple crack model is related to β_i, $\bar{\sigma'}_{1k} = C_{kl}\beta_l$. Here, the origin of the coordinate system, $\bar{x}_1$,$\bar{x}_2$ lies at the center of the ellipse with $\bar{x}_2$ directed along the major axis (Figure 1). Writing the crack face displacement in terms of the coordinate system with the origin placed at the crack tip (Figure 2),

$$\bar{U}_i' = \beta_i\sqrt{2\bar{a}\tilde{\zeta}} \tag{29}$$

where $\tilde{\zeta}$ is the distance from the crack tip along $\tilde{x}_2$. Comparing (28) with (29) we get

$$\mathbf{Q}^{-1}\bar{\mathbf{K}} = [\beta]\sqrt{\pi\bar{a}}. \tag{30}$$

which relates the unknowns, $\bar{\mathbf{K}}$ and $[\beta]$. In order to complete the problem, we determine the elastic energy released from the simple crack model,

$$\bar{\xi} = 2\frac{1}{2}\int_{-\bar{a}}^{\bar{a}} \bar{\sigma}_{1k}^{o}\bar{U}_k \mathrm{d}\tilde{x}_2 = -C_{ik}\beta_i\beta_k\frac{\pi\bar{a}^2}{2} \tag{31}$$

and equate $\frac{\mathrm{d}\bar{\xi}}{\mathrm{d}\bar{a}} = 2\bar{J}$ giving,

$$\bar{K}_i = \sqrt{\pi\bar{a}}\bar{\sigma}_{1j}^{o} \tag{32}$$

where $\bar{J}$ is value of the standard J-integral,[21] determined in the limit as the integration path is shrunk so as to lie along the crack face,

$$\bar{J} = \lim_{\delta\to 0}\frac{1}{\delta}\int_0^{\delta} \bar{\sigma'}_{1i}(\delta - \tilde{r}, -\frac{\pi}{2})\bar{u}_i'(\tilde{r}, \frac{\pi}{2})\mathrm{d}\tilde{r} = -\frac{1}{2}\bar{K}_i\left(Q_{il}^{-1}\bar{K}_l\right). \tag{33}$$

Comparing (30) and (32) gives the expression for β_i in terms of the far field stresses,

$$\beta_i = \mathbf{Q}_{ik}^{-1} \bar{\sigma^{\mathbf{o}}}_{1k}.$$

We are now in a position to write the elastic energy recovered (dimensional) due to the formation of a finite length mode-I crack of length a,

$$\xi = -\frac{\pi}{2} a^2 Q_{11}^{-1} \frac{(\sigma_{11}^o)^2}{E} \tag{34}$$

The present problem requires the crack surface to be have a normal stress ($-\bar{\sigma^o}_{11}$) and the far field perturbed stress to be zero. Consequently, the complex stress function $G_k(z_k)$ in (21) is replaced with $G_k(z_k) + \Gamma_k z_k$ $(k = 1, 2)$, where Γ_k are real constants[19]. Substituting the new expression for G_k and applying the traction boundary condition at the crack surface, we get,

$$\begin{bmatrix} \Gamma_1 \\ \Gamma_2 \end{bmatrix} = \mathbf{Re} \left\{ \frac{1}{\mu_1 \mu_2 (\mu_1 - \mu_2)} \begin{bmatrix} \mu_2 & \mu_2^2 \\ \mu_1 & \mu_1^2 \end{bmatrix} \begin{bmatrix} -\bar{\sigma^o}_{11} \\ 0 \end{bmatrix} \right\} \tag{35}$$

The above expression along with the definition for the stresses (21) suggests that both $\bar{\sigma'}_{11}$ and $\bar{\sigma'}_{22}$ are influenced by the traction condition. However, neither $\bar{\sigma'}_{12}$ nor $\bar{u}_1'$ along the crack face are effected implying that the energy calculations and the corresponding values of the stress intensity factors remain unchanged.

The total energy for the system is $\mathcal{E} = \xi + \Gamma$, where $\Gamma = 4\gamma a$ corresponds to surface energy and γ is the surface tension. Following Griffith's argument,[23] the crack will be in equilibrium when,

$$\frac{\mathrm{d}\mathcal{E}}{\mathrm{d}a} = 0 \Rightarrow \sigma_{11}^o = \sqrt{\frac{4\gamma E}{Q_{11}^{-1} a \pi}} \tag{36}$$

which relates the far field stress to the crack length and surface tension. Since E is a linear function of the pre-crack strain which in turn is related to the far field stress, we have

$$\sigma_{11}^o (a)^{2/3} = \left[\frac{2\gamma}{Q_{11}^{-1} \pi} \right]^{2/3} \left(\frac{GM\phi_{rcp}}{35} \right)^{1/3} \tag{37}$$

A more useful relation is in terms of the capillary pressure,

$$\left(-\frac{P^o R}{2\gamma}\right)\left(\frac{a}{R}\right)^{2/3} = \left\{\frac{3}{4}\left[\frac{8}{35 Q_{11}^{-2}\pi^2}\right]^{1/3}\right\}\left(\frac{GM\phi_{rcp}R}{2\gamma}\right)^{1/3}. \tag{38}$$

Thus the dimensionless critical capillary pressure is related to the dimensionless crack length,

$$(-\tilde{P}^o)(\tilde{a}^{2/3}) = AW^{1/3} \tag{39}$$

where, $W = GM\phi_{rcp}R/2\gamma$ represents the balance of the elastic and surface energy and A is equal to 0.45 and 0.35 for the short and long time limit, respectively.

4 Numerical solution

The stress and the displacement field obtained in the previous section is applicable to regions close to the crack tip. For the full solution, the momentum balance equation (10) for the perturbed stresses were solved numerically for the control volume highlighted in Figure 1 using finite element method (DIFFPACK®). The boundary conditions are as follows,

$$\begin{aligned}
\bar{\sigma'}_{11} &= -\bar{\sigma}^o_{11} && \text{for } \bar{x}_1 = 0, 0 > \bar{x}_2 > -\bar{a},\\
\bar{u}'_1 &= 0 && \text{for } \bar{x}_1 = 0, -\tilde{a} > \bar{x}_2 > -1,\\
\bar{u}'_2 &= 0 && \text{for } 0 < \bar{x}_1 < 1, \bar{x}_2 = 0,\\
\bar{\sigma'}_{22} &= 0 && \text{for } 0 < \bar{x}_1 < 1, \bar{x}_2 = -1, \text{ and}\\
\bar{\sigma'}_{11} &= 0 && \text{for } \bar{x}_1 = 1, 0 > \bar{x}_2 > -1
\end{aligned}$$

where $\bar{a} << 1$ so that the stress and the strain fields close to the crack are not influence by the size of the control volume.

Rectangular elements were used with adaptive refinement of the grid near the crack tip. The total number of nodes in the control volume were about 50,000.

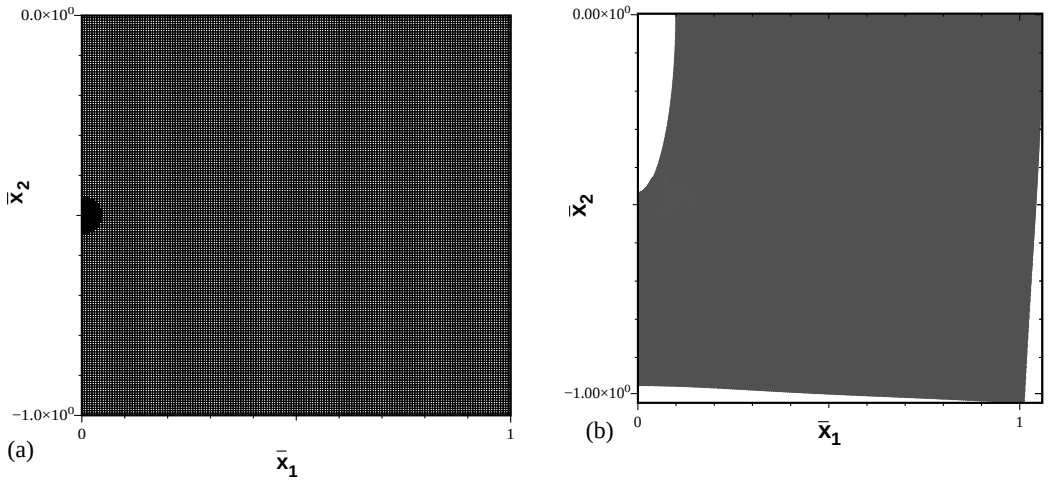

Figure 3: (b) The basic grid before deformation. (b) The scaled surface deformation of the control volume for the short time limit. All displacements have been scaled with one-tenth the maximum displacement ($u_1'(0,0)$).

5 Results and Discussion

5.1 Numerical Simulation

The perturbed stress, strain and displacements obtained from the numerical simulations are presented in Figure 3, 4, 5. Unless specified, all results pertain to the short time limit. Figure 3(a) and (b) presents the initial and deformed grid, respectively. The surface displacements in Figure 3(b) have been scaled so as to highlight their magnitude. As expected, the displacement at the center of the crack is maximum with the tip of the crack moving upwards. Since the perturbed stresses are zero at the control volume boundaries, the effect of the surface displacement at the crack faces can be observed at the boundaries. The equilibrium shape of the crack surface is elliptical and ratio of the length of the minor to major axis is very small ($\sim 10^{-3}$), both of which are in agreement with the asymptotic solution. Figure 4 presents the simulated values of $\bar{\sigma'}_{11}$ and $\bar{\sigma'}_{22}$ for the control volume. The contour plot (Figure 4(a) and (c)) and the gray scale plots of the region close to the crack tip (Figure 4(b) and (d)) demonstrate the sharp decrease in stress with increasing distance from

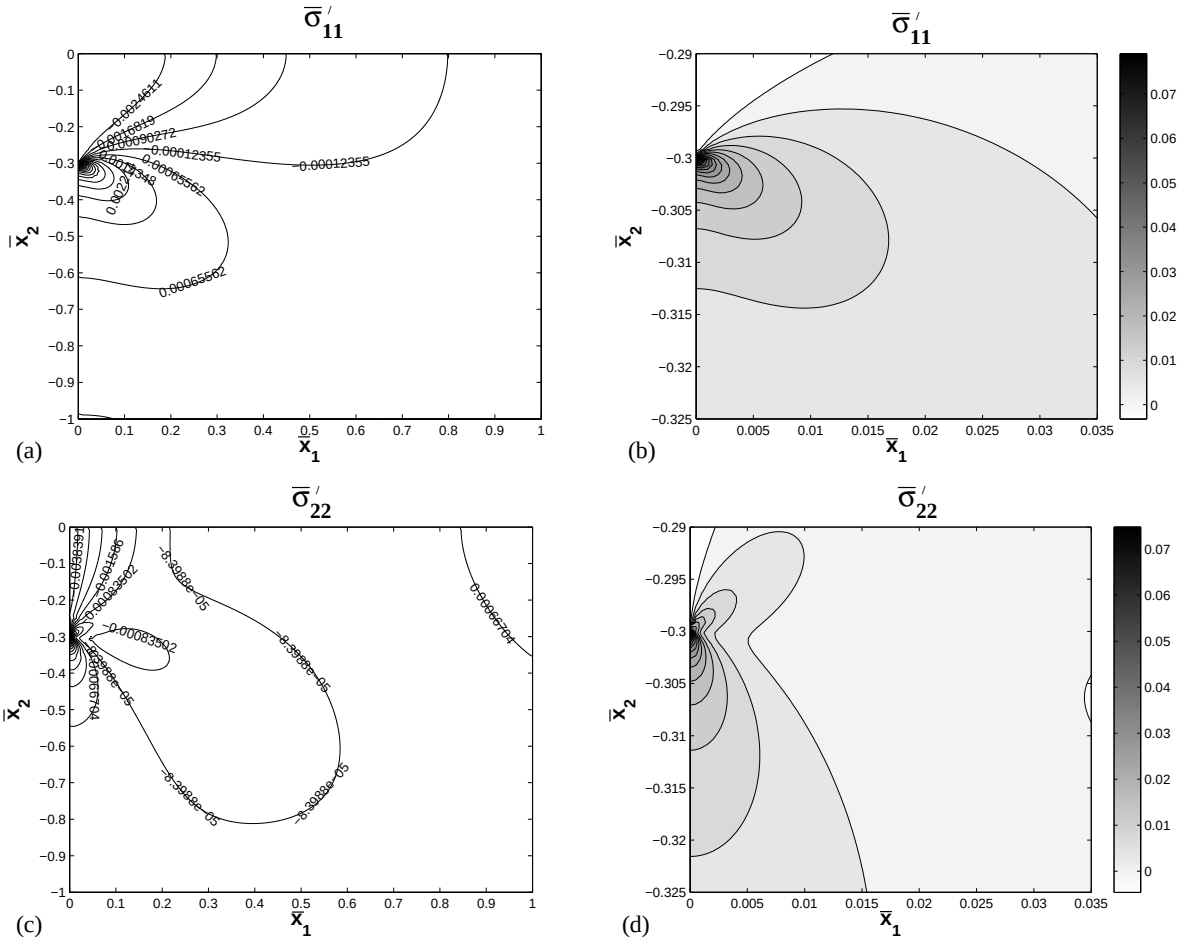

Figure 4: Variation of perturbed stresses for nondimensional half crack length, $\bar{a} = 0.3$ and $\epsilon^o = 7.8 \times 10^{-4}$: (a) Contour plot of $\bar{\sigma'}_{11}$, (b) Gray scale plot of $\bar{\sigma'}_{11}$ close to crack tip, (c) contour plot of $\bar{\sigma'}_{22}$, and (c) Gray scale plot of $\bar{\sigma'}_{11}$ close to crack tip.

the crack tip. The contours are perpendicular to the symmetry surfaces ($\bar{x}_2 = 0$ and $-0.3 < \bar{x}_1 < 1, \bar{x}_2 = 0$) as expected from the boundary conditions while they decay to zero at $\bar{x}_1 = 1$ and $\bar{x}_2 = -1$. Figure 5(a) and (b) present the perturbed pressure for the short time limit. Interestingly, the pressure is negative close to the tip suggesting that the solvent will flow towards the tip once the crack nucleates. This is borne out in the simulations for the long time limit (Figure 5(c) and (d)) where the particle concentration has reduced at the tip. Note that while the particle concentration should always be equal or more than the close pack concentration at

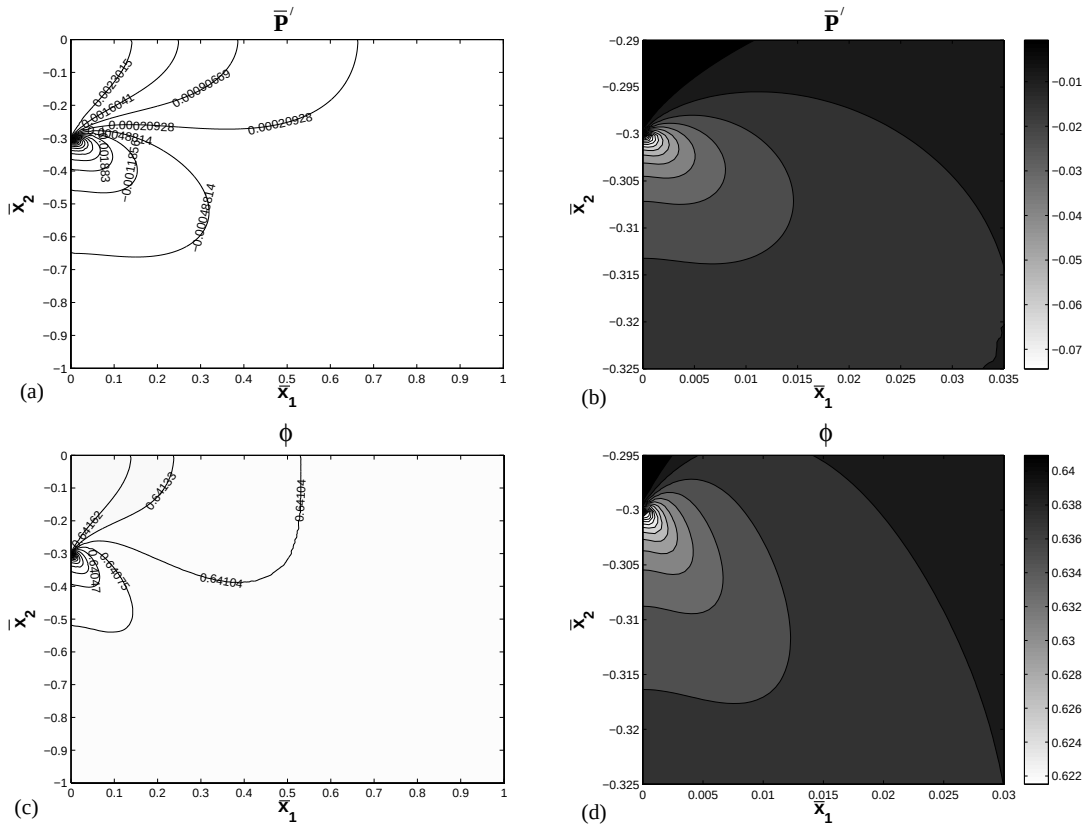

Figure 5: Variation of perturbed pressure in the short time limit for $\bar{a} = 0.3$: (a) Contour plot of $\bar{P}'$, (b) Gray scale plot of $\bar{P}'$ close to crack tip. Variation of the particle concentration in the long time limit: (c) Contour plot of ϕ, and (d) Gray scale plot of ϕ close to crack tip.

all times, values of $\phi < \phi_{rcp}$ near the crack tip in the long time limit are not physical since no such constraint has been imposed in the simulation. Instead, extra solvent could accumulate at the crack tip between the crack faces.

5.2 Comparison with Asymptotic Solution

Figure 6 compares the spatial variation of perturbed displacement, $\bar{u}_1'$, along the crack face obtained from the simulation with that predicted by the asymptotic solution. At the crack tip, $\bar{u}_1' = 0$ while for $10^{-4} < \bar{x}_1 < 10^{-2}$, the displacement varies as the square root of the distance from the tip. The disagreement close to and far away from the crack tip is attributed to the limitation on grid refinement in case of

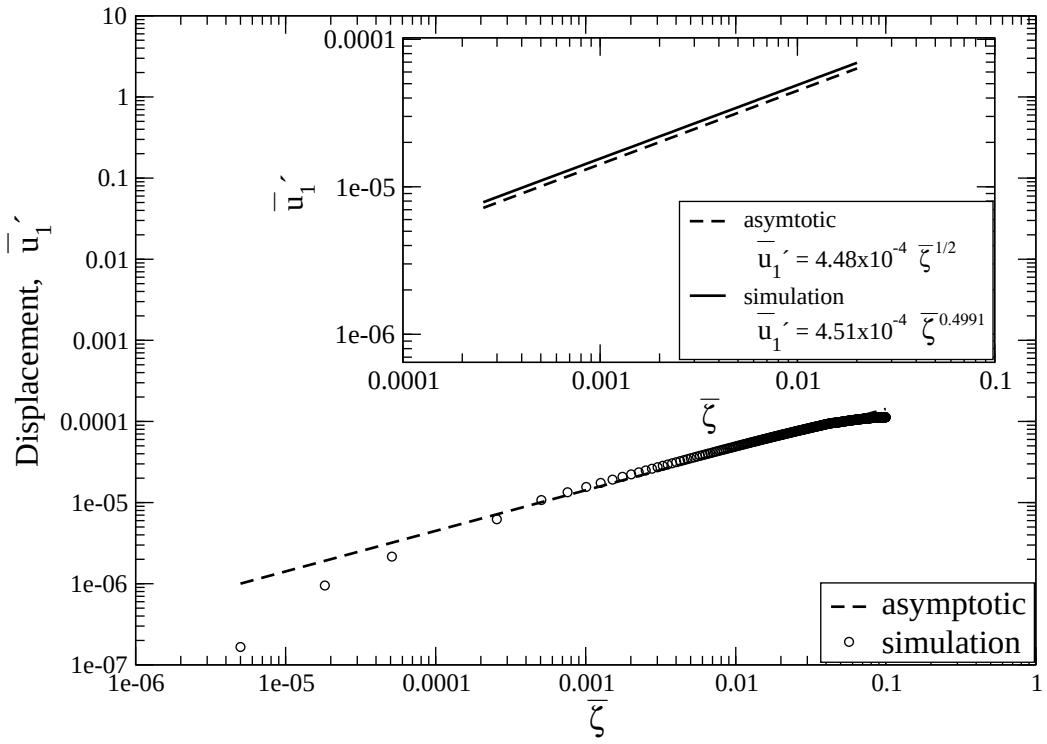

Figure 6: Displacement $\bar{u}_1'$ for $\bar{a} = 0.3$ along the crack face.

numerical solution close to the tip (which is unable to capture the large variations in the stress) and to the non-applicability of the asymptotic solution far away from the crack tip. Figure 7 presents the spatial variation of $\bar{\sigma}'_{11}$ along $\bar{x}_1$ away from the crack tip for $\bar{a} = 0.3$. As expected the stress diverges as $\bar{x}_1^{-\frac{1}{2}}$ close to the crack tip and the prediction matches well with the numerical solution for $10^{-4} < \bar{x}_1 < 10^{-2}$. Far away from the crack tip, the perturbed stresses vanish. The angular distribution of stresses obtained from the asymptotic solution agrees with that from the numerical solution in Figure 8 at $|\bar{r} - \bar{a}| = 0.012\cdot$ The distribution is somewhat similar to that obtained for the isotropic cases.[26] Figure 9 compares the angular distribution of the stresses at various radial distances from the crack tip, both in the short and the long time limits. The magnitude of the stresses at a given location in the long time limit are lower than those in the short time limit. This decrease may be attributed to the flow of the solvent that relieves any pressure variation that develops in the short time

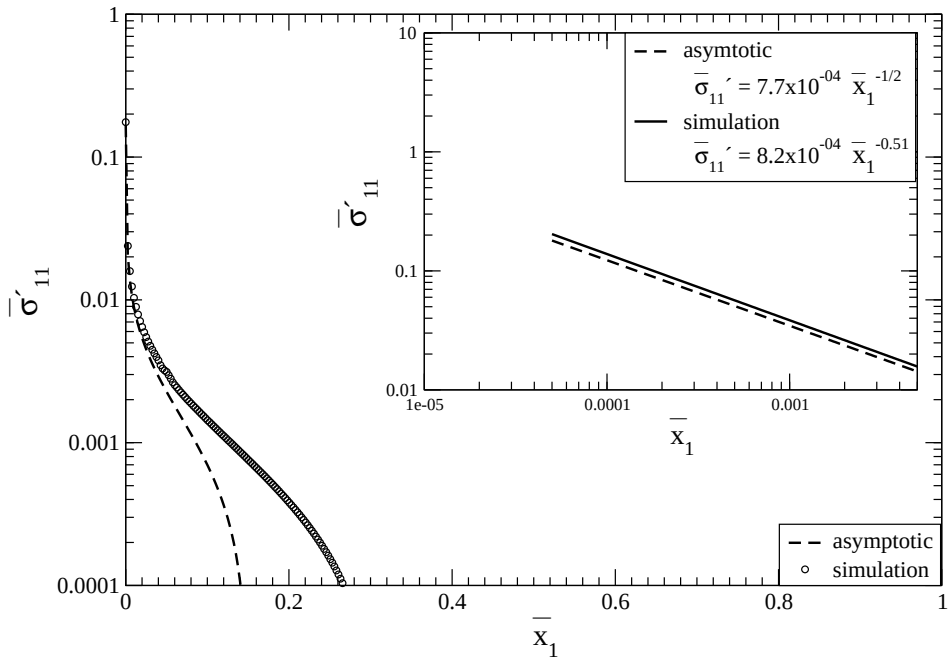

Figure 7: Perturbed stress $\bar{\sigma'}_{11}$ along $\bar{x}_1$ ($\bar{x}_2 = -\bar{a}$) for $\bar{a} = 0.3$.

limit. Compared to the short time limit, the angular variation of the stress in the long time limit show larger deviations from the isotropic case as also suggested by the values of δ_i in (15).

The Griffith's criteria (39) shows that the pressure required to open a crack increases with decreasing size of the crack. Since the maximum dimensionless capillary pressure is about[27] 5.3, the largest allowable flaw which will not crack the sample is, $\tilde{a}_{\max} = 0.025\sqrt{W}$ which suggests that packings containing particles of larger size and/or higher shear moduli can resist cracking more effectively. Recently, Tirumkudulu and Russel[3] have derived the expression for the critical capillary stress to drive an infinite crack through a drying colloidal thin film bound to a substrate, $(-\tilde{P}^o_\infty)(\tilde{h}^{2/3}) = 0.23W^{1/3}$. Comparing the critical capillary pressure for the two cases suggests that when $\tilde{a} \ll \tilde{h}$, a significantly larger capillary pressure is required to expand a finite flaw in the film compared to that required to drive an infinite crack,

$$\frac{\tilde{P}^o}{\tilde{P}^o_\infty} \sim \left(\frac{\tilde{h}}{\tilde{a}}\right)^{\frac{2}{3}}.$$

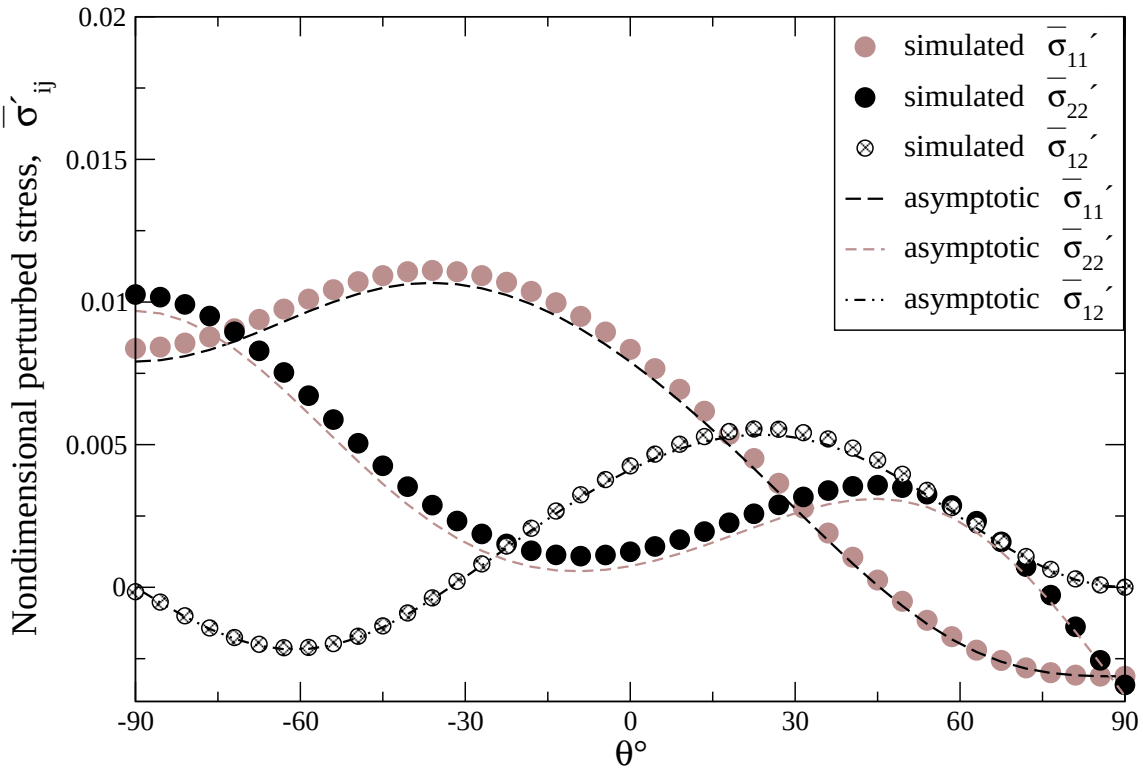

Figure 8: Angular variation of perturbed stresses for short time at $|\bar{r} - \bar{a}| = 0.012$ for $\bar{a} = 0.1$.

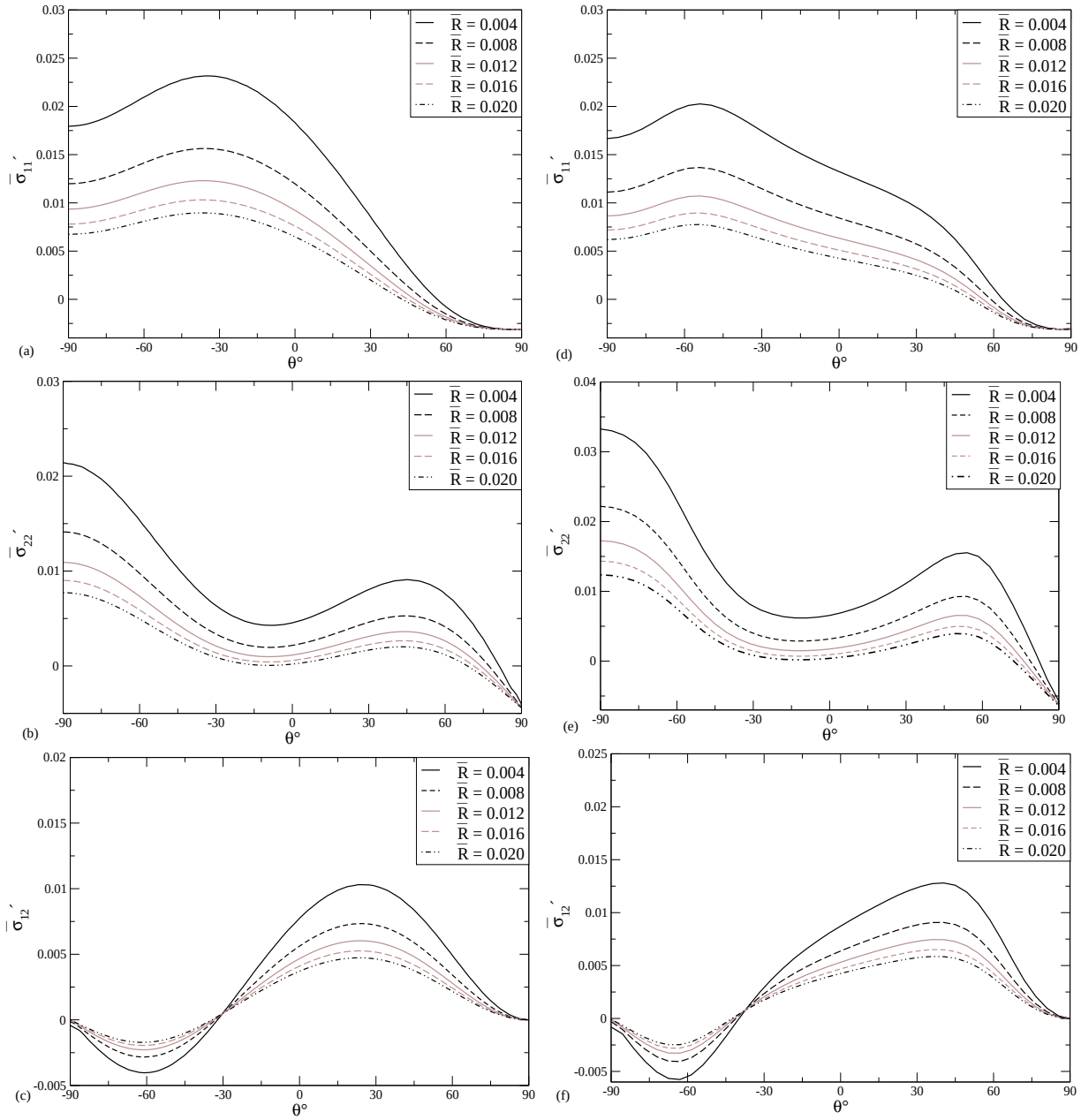

Figure 9: Angular variation of perturbed stresses at different radii ($\bar{R} = \bar{r} - \bar{a}$), (a)–(c) in the short time limit, and (d)–(f) in the long time limit for $\bar{a} = 0.3$.

The above result also indicates that the maximum crack free thickness for the thin colloidal film is obtained when the maximum allowable flaw size for a crack free film is of a similar magnitude, $\tilde{h}_{\max} \sim \tilde{a}_{\max}$. These results are in line with the recent theoretical results obtained by Russel et al.[17] using the more accurate constitutive relation and experiments measuring the critical capillary pressure for various particle packings.[18]

The energy release rate, $\mathcal{G} = 2J$, is related to the stress intensity factor through the standard relation, $\mathcal{G} = \frac{K^2}{E_{\text{eff}}}$ where the effective elastic modulus for the packing,

$$E_{\text{eff}} = \frac{E}{Q_{11}^{-1}} \ , \tag{40}$$

accounts for the particle size and packing, and also for the anisotropy resulting from the nucleation of crack.

Finally the analysis presented here is general, in that the results relating to the asymptotic forms of the stress and displacement component, and the related expression for the energy release rate can easily be obtained for any other constitutive equation once the stiffness matrix for the linearized equation is known.

6 Conclusions

We present the asymptotic analysis of the deformation field near a crack tip for a mode I crack in a two dimensional colloidal packing saturated with solvent. The stress and strain fields are linearized about the pre-crack state to yield the stress intensity factor for the two dimensional elastic field which is then related to the surface energy using the well known Griffith's criterion for equilibrium cracks. The calculated quantities are then compared with the numerical solution for the full problem. The results show that the dimensionless critical capillary pressure required to open a crack varies inversely with the crack length to the two thirds' power and is controlled by the ratio of the elastic energy stored in the packing and the increase in surface energy due to

crack nucleation. The analysis also gives the maximum flaw size to achieve a crack free packing.

References

[1] Martinez, C. J.; Lewis, J. A. *J. Am. Ceram. Soc.* **2002**, *85*, 2409–2425.

[2] Egen, M.; Zentel, R. *Chem. Mater.* **2002**, *14*, 2176–2183.

[3] Tirumkudulu, M. S.; Russel, W. B. *Langmuir* **2005**, *21*, 4938 – 4948.

[4] Petersen, C.; Heldmann, C.; Johannsmann, D. *Langmuir* **1999**, *15*, 77457751.

[5] Chiu, R. C.; Garino, T. J.; Cima, M. J. *J. Am. Ceram. Soc.* **1993**, *76*, 2257 – 2264.

[6] Chiu, R. C.; Cima, M. J. *J. Am. Ceram. Soc.* **1993**, *76*, 2769 – 2777.

[7] Singh, K. B.; Bhosale, L. R.; Tirumkudulu, M. S. *Langmuir* **2009**, *25*, 4284–4287.

[8] Shorlin, K. A.; de Bruyn, J. R.; Graham, M.; Morris, S. W. *Phys. Rev. E* **2000**, *61*, 6950–6957.

[9] Allain, C.; Limat, L. *Phys. Rev. Lett.* **1995**, *74*, 2981–2984.

[10] Goehring, L.; Mahadevanb, L.; Morris, S. W. *Proc. Natl. Acad. Sci. U.S.A.* **2009**, *106*, 387392.

[11] Dufresne, E. R.; Corwin, E. I.; Greenblatt, N. A.; Ashmore, J.; Wang, D. Y.; Dinsmore, A. D.; Cheng, J. X.; Xie, X. S.; Hutchinson, J. W.; Weitz, D. A. *Phys. Rev. Lett.* **2003**, *91*, 224501.

[12] Routh, A. F.; Russel, W. B. *Langmuir* **1999**, *15*, 7762 – 7773.

[13] Biot, M. A. *J. Applied Phys.* **1941**, *12*, 155–164.

[14] Biot, M. A. *J. Applied Phys.* **1955**, *26*, 182–185.

[15] Biot, M. A. *J. Applied Phys.* **1956**, *27*, 459–467.

[16] Tirumkudulu, M. S.; Russel, W. B. *Langmuir* **2004**, *20*, 2947 – 2961.

[17] Russel, W. B.; Wu, N.; Man, W. *Langmuir* **2008**, *24*, 1721 – 1730.

[18] Man, W.; Russel, W. B. *Phys. Rev. Lett.* **2008**, *100*, 198302.

[19] Sih, G. C.; Paris, P. C.; Irwin, G. R. *International Journal of Fracture* **1965**, *1*, 189–203, 10.1007/BF00186854.

[20] Lekhnitskii, S. G. *Theory of an Anisotropic Elastic Body (translated by P. Fern)*; Mir Publishers: Moscow, 1981.

[21] Rice, J. R. *Journal of Applied Mechanics* **1968**, *35*, 379 – 386.

[22] Eshelby, J. D. *Proceedings of the Royal Society of London. Series A, Mathematical and Physical Sciences* **1957**, *241*, pp. 376–396.

[23] Griffith, A. *Proc. R. Soc. A* **1921**, *221*, 163 – 198.

[24] Hoenig, A. *Engineering Fracture Mechanics* **1982**, *16*, 393 – 403.

[25] Eshelby, J. D. *Proc. Roy. Sot. London,Series A* **1957**, *241*, 376 – 396.

[26] Lawn, B. *Fracture of Brittle Solids*, 2nd ed.; Cambridge University Press: United Kingdom, 1993.

[27] Mason, G.; Mellor, D. W. *J. Colloid Interf. Sci.* **1995**, *176*, 214–225.